frontiers in Materials

ORIGINAL RESEARCH
published: 31 October 2018
doi: 10.3389/fmats.2018.00063

The Recovery of the Waste Cigarette Butts for N-Doped Carbon Anode in Lithium Ion Battery

Chengyi Yu[1], Hongying Hou[1], Xianxi Liu[2]*, Lina Han[1], Yuan Yao[1], Zhipeng Dai[1] and Dongdong Li[1]*

[1] Faculty of Material Science and Engineering, Kunming University of Science and Technology, Kunming, China, [2] Faculty of Mechanical and Electronic Engineering, Kunming University of Science and Technology, Kunming, China

As one of the common life garbages, about 4.5 trillion waste cigarette butts are produced and randomly discarded every year due to the addiction to the nicotine and the need of the social intercourse. Such a treatment would result in the waste of the resources and the environmental pollution if they weren't reasonably recycled in time. Herein, the waste cigarette butts were recycled in form of N-doped carbon powders with high economic value-added via one-step facile carbonization at 800°C for 2 h in the inert N_2 atmosphere. The waste-cigarette-butts-derived black carbon powders were characterized by scanning electron microscope (SEM), N_2 adsorption/desorption, and X-ray photoelectron spectroscopy (XPS). Furthermore, the corresponding electrochemical performances as the anode in lithium ion battery (LIB) were also investigated by galvanostatic charge/discharge, cyclic voltammetry (CV), and alternating current (AC) impedance. The results suggested that the recycled N-doped waste cigarette butts carbon (WCBC) powders consisted of major carbon and minor residual N-containing and O-containing functional groups, and the corresponding specific surface area was about 1,285 $m^2 \cdot g^{-1}$. Furthermore, the reversible specific discharge capacity was about 528 $mAh \cdot g^{-1}$ for 100 cycles at 25 $mA \cdot g^{-1}$ and about 151 $mAh \cdot g^{-1}$ even at 2,000 $mA \cdot g^{-1}$ for 2,500 cycles. Additionally, full cell performances were also satisfactory, indicating high feasibility. N-doping effect (such as additional active sites and higher electronic conductivity) and the residual O-containing functional groups may be responsible for the satisfactory electrochemical performances, which offered good inspiration and strategy to develop the green energy and circular economy.

Keywords: waste cigarette butts, recovery, N-doped carbon, lithium ion battery, anode

OPEN ACCESS

Edited by:
Jie-Sheng Chen,
Shanghai Jiao Tong University, China

Reviewed by:
Yong Chen,
Hainan University, China
Leszek A. Czepirski,
AGH University of Science and Technology, Poland

***Correspondence:**
Hongying Hou
hongyinghou@kmust.edu.cn
Xianxi Liu
xxiliu@tom.com

Specialty section:
This article was submitted to Carbon-Based Materials, a section of the journal Frontiers in Materials

Received: *20 August 2018*
Accepted: *12 October 2018*
Published: *31 October 2018*

Citation:
Yu C, Hou H, Liu X, Han L, Yao Y, Dai Z and Li D (2018) The Recovery of the Waste Cigarette Butts for N-Doped Carbon Anode in Lithium Ion Battery. Front. Mater. 5:63. doi: 10.3389/fmats.2018.00063

INTRODUCTION

According to the World Health Organization's statistics in 2012, there existed about 1.1 billion smokers in the world (Islami et al., 2015). As is known to all, although the smoking is harmful to the health, it is difficult to quit smoking due to the addiction to the nicotine and the need of the social intercourse, resulting in the production and large accumulation of the countless waste cigarette butts (Jarvis, 2004). It was reported that about 4.5 trillion waste cigarette butts were randomly discarded as one of the common life garbages every year worldwide (Slaughter et al., 2011). The waste cigarette butts are ubiquitous in the environment, as shown in **Figure 1**, which would cause

the environment pollution and the waste of the resources if they weren't reasonably recycled in time. For example, the leachate from the waste cigarette butts can seriously affect the survival of the aquatic organisms, as reported elsewhere (Slaughter et al., 2011).

Generally, one waste cigarette butt consists of three parts: the filter tip, the remnant tobacco and the packing paper (Slaughter et al., 2011). As one main part of the waste cigarette butt, the filter tip is made up of the cellulose acetate, which can protect the smoker by absorbing the various carcinogenic constituents within the cigarette such as the tar, nicotine, hydrogen cyanide, and benzopyrene (Hoffmann and Hoffmann, 1997; Smith and Novotny, 2011). And the packing paper and the remnant tobacco also contain the rich cellulose. Generally, the waste cigarette butts into the environment are subjected to the incineration and the landfill together with other common life garbages, which may result in the waste of the useful resources and the potential environment pollution. Therefore, it is imperative to explore the reasonable reutilization of the waste cigarette butts. Considering that the main component of the waste cigarette

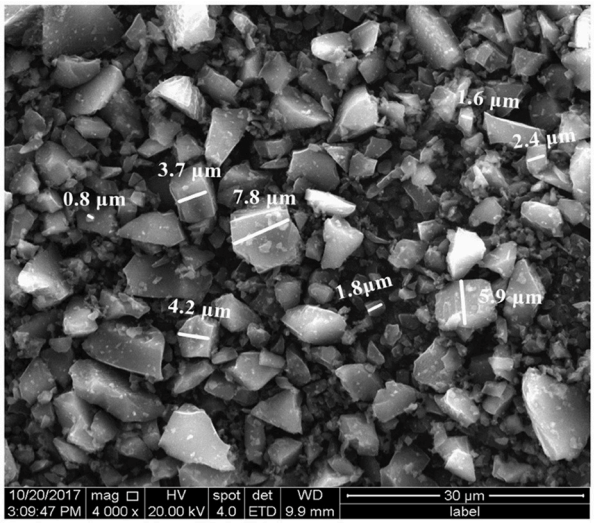

FIGURE 3 | SEM image of N-doped WCBC powders.

FIGURE 1 | The ubiquitous waste cigarette butts in the environment: **(a)** scrap heap, **(b)** tree well, **(c)** street corner, **(d)** puddle, **(e)** roadside and **(f)** wasteland (Guernsey Police, 2013; Woods, 2015).

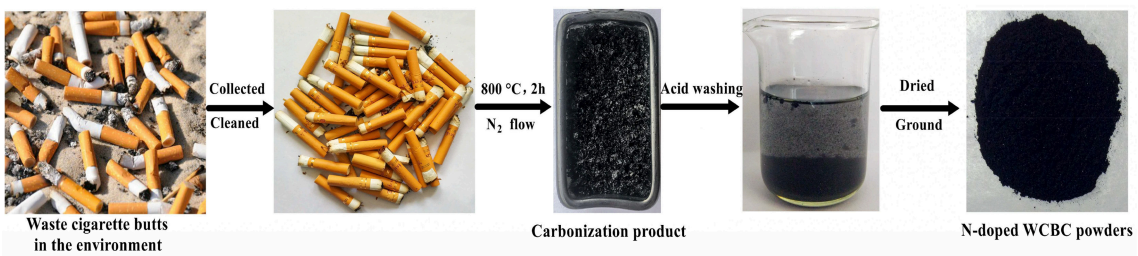

FIGURE 2 | The recycled procedures of the waste cigarette butts.

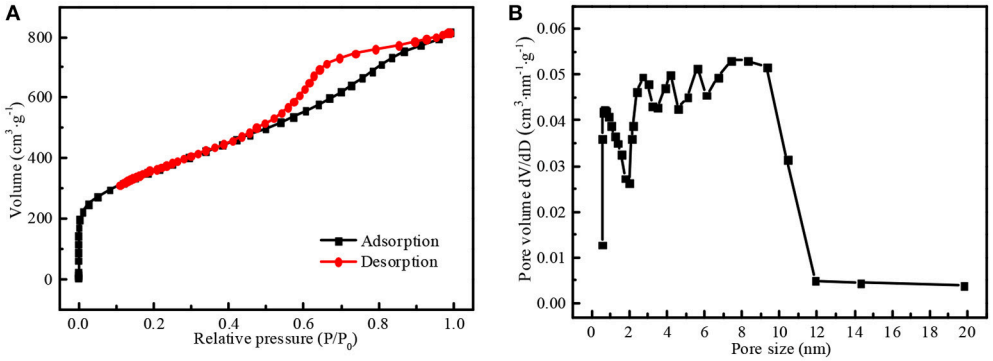

FIGURE 4 | (A) N_2 adsorption/desorption isotherms and **(B)** the pore size distribution curve of N-doped WCBC powders.

butt is the organic carbon-rich cellulose, the waste cigarette butts may be reasonably recycled in the form of high economic value-added carbon powders, which will not only alleviate the potential environmental pollution but also promote the circular economy and the sustainable development. However, there are few reports about the recovery of the waste cigarette butts for the moment.

Currently, some energy storage and conversion devices such as lithium ion battery (LIB), sodium ion battery, fuel cell, and supercapacitor attracted much attention, among which LIB has rapidly captured the market of the portable devices and the electric vehicles due to the long cycle life span and environmental friendliness since its commercialization in 1990s (Li et al., 2014, 2015; Luo et al., 2015; Dai et al., 2016; Liu et al., 2016a; Tie et al., 2018; Yu et al., 2018). As we know, it is the application of carbon-based anode that achieved such a huge success of LIB due to low cost, good electrical conductivity, stable physicochemical property. N-doping can further enhance the electrochemical performances of carbon anode due to the following N-doping effect such as high electrical conductivity, the formation of the structural defects and additional Li-storage active sites (Bulusheva et al., 2011; Song et al., 2014; Zheng et al., 2014). Firstly, N atoms within the graphitic matrix can act as the electron donors and increase the local state density at Fermi level, and thus enhance the electrical conductivity (Royea et al., 2006; Wiggins-Camacho and Stevenson, 2009). Secondly, several different combinations of N with C such as pyridinic N and pyrrolic N may act as the additional active sites for Li-storage (Bhattacharjya et al., 2014). Additionally, N-doping may also induce the formation of some defect spaces for the additional active sites to storage Li^+. For example, it was reported that N-doping can increase the reversible discharge capacity of carbon anode from 250 to 535 $mAh{\cdot}g^{-1}$ at 20 $mA{\cdot}g^{-1}$ after 200 cycles (Han et al., 2012). Generally, N-doping of carbon material can be achieved via the hydrothermal route, the ultrasonication or the electrochemistry, among which *in situ* carbonization of N-containing carbon precursors may be preferable because the uniform distribution of N atom can be achieved (Stephan et al., 1994; Saravanan and Kalaiselvi, 2015). Considering that both nicotine and hydrogen cyanide within the waste cigarette butts belong to N-containing compounds, the waste cigarette butts containing the rich cellulose may be a preferable precursor of N-doped carbon material.

Herein, in this work, the waste cigarette butts were recycled by one step facile carbonization at 800°C for 2 h in the inert N_2 atmosphere. Furthermore, N-doped WCBC anode in LIB exhibited high specific capacity and cycling stability. Furthermore, in order to further investigate the feasibility of N-doped WCBC anode, a full cell was also assembled and tested by coupling N-doped WCBC anode with commercial $LiCoO_2$ cathode. It is very instructive to build the bridge between the waste resources and the clean energy materials, especially for the toxic wastes.

EXPERIMENTAL

The Recovery of the Waste Cigarette Butts

After some waste cigarette butts were collected and cleaned, they were recycled in form of black N-doped carbon powders via one step facile carbonization, as shown in **Figure 2**. Briefly, after being cleaned and cut into small pieces, the waste cigarette butts were carbonized at 800°C in a tubular furnace for 2 h at $5°C{\cdot}min^{-1}$ under N_2 flow. Then, the obtained black carbon powders were immersed in 10% HCl aqueous solution for 24 h at room temperature to remove the inorganic impurities and then washed with the distilled water. Finally, the clean black carbon powders were obtained after being dried and fully ground.

Structure and Morphology Characterization

The morphology of the sample was probed by SEM (Quanta200 FEI, USA). The corresponding surface area and pore volume were determined by specific surface and pore size analysis instrument (V-Sorb 2800TP Gold APP, China), and the chemical component was characterized by XPS technology on X-ray photoelectron spectrometer (PHI5000 Versaprobe-II ULVAC-PHI, Japan).

Electrochemical Measurements

The procedures to fabricate the electrode and assemble the coin cell were described as follows. Firstly, the electrode slurry was prepared by fully mixing 80 wt% active material, 10 wt% acetylene

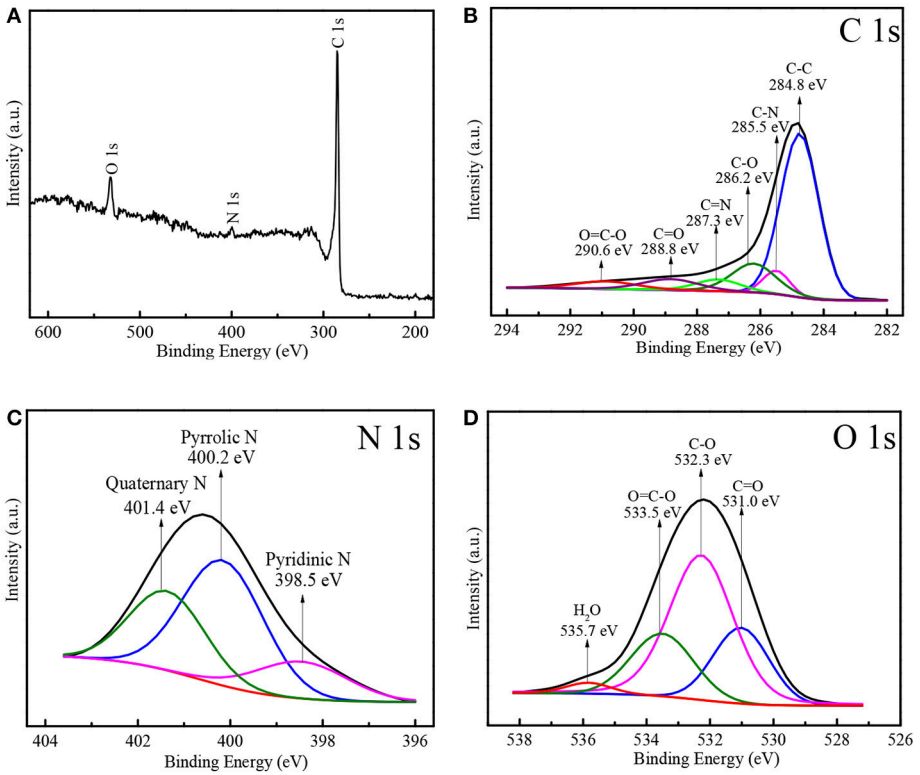

FIGURE 5 | XPS spectra of N-doped WCBC powders: **(A)** the wide scan **(B)** C 1s, **(C)** N 1s, and **(D)** O 1s.

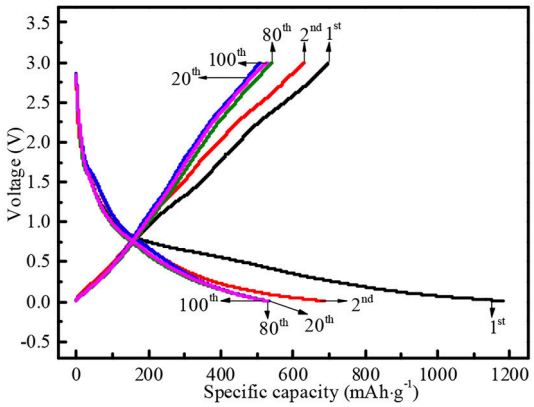

FIGURE 6 | The 1st, 2nd, 20th, 80th, and 100th galvanostatic charge/discharge profiles of N-doped WCBC anode at 25 mA·g^{-1}.

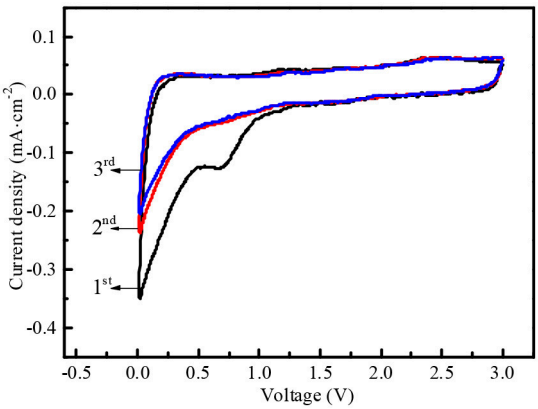

FIGURE 7 | CV curves of N-doped WCBC anode at different cycles.

black, and 10 wt% PVDF binder in N-methyl-2-pyrrolidone. Secondly, N-doped WCBC anode and $LiCoO_2$ cathode can be obtained by coating the electrode slurries onto Cu foil and Fe foil, respectively, and vacuum dried at 60°C for 12 h. The loading densities of N-doped WCBC and $LiCoO_2$ were about 1.1 and about 2.8 mg·cm^{-2}, respectively. CR2032 coin cell was assembled in an argon-filled glove box (Mikrouna Super 1220/750/900), in which N-doped WCBC anode was coupled with the counter electrodes of Li foil and $LiCoO_2$ cathode in half and full cell, respectively, and the electrolyte was 1 M $LiPF_6$ in ethylene carbonate and diethyl carbonate (1:1 in volume), and the commercial porous Celgard 2400 film was the separator (Hou et al., 2018). The coin cell was evaluated by galvanostatic charge/discharge on a battery testing system (Neware CT-3008W, China) at 25, 1,000, and 2,000 mA·g^{-1}. The electrochemical performances were further carried out by cyclic voltammetry (CV) curve (0.01−3.0 V at 0.2 mV·s^{-1}) and AC impedance

(0.01 Hz−100 kHz, 10 mV perturbation) on the electrochemical workstation (Parstat 4000, Princeton Applied Research, USA).

RESULTS AND DISCUSSION

SEM

The micro-morphology of N-doped WCBC powders was probed by SEM, as shown in **Figure 3**. Clearly, N-doped WCBC powders were made up of many irregular micro-particles with the particle size of about 0.8–7.8 μm, which may endow N-doped WCBC powders with high surface area and facilitate the sufficient infiltration of the electrolyte into the electrode (Jiang et al., 2016).

Nitrogen Adsorption/Desorption Analysis

N_2 adsorption/desorption isotherms of N-doped WCBC powders were recorded by static volumetric method (also known as manometric method), which exhibited the features of type IV curve, as shown in **Figure 4A** (Thommes et al., 2015; Qin and Chen, 2017). Specifically, the adsorption volume steeply increased at the range of $P/P_0 < 0.01$ and an obvious hysteresis loop appeared at the range of $P/P_0 > 0.45$, indicating the

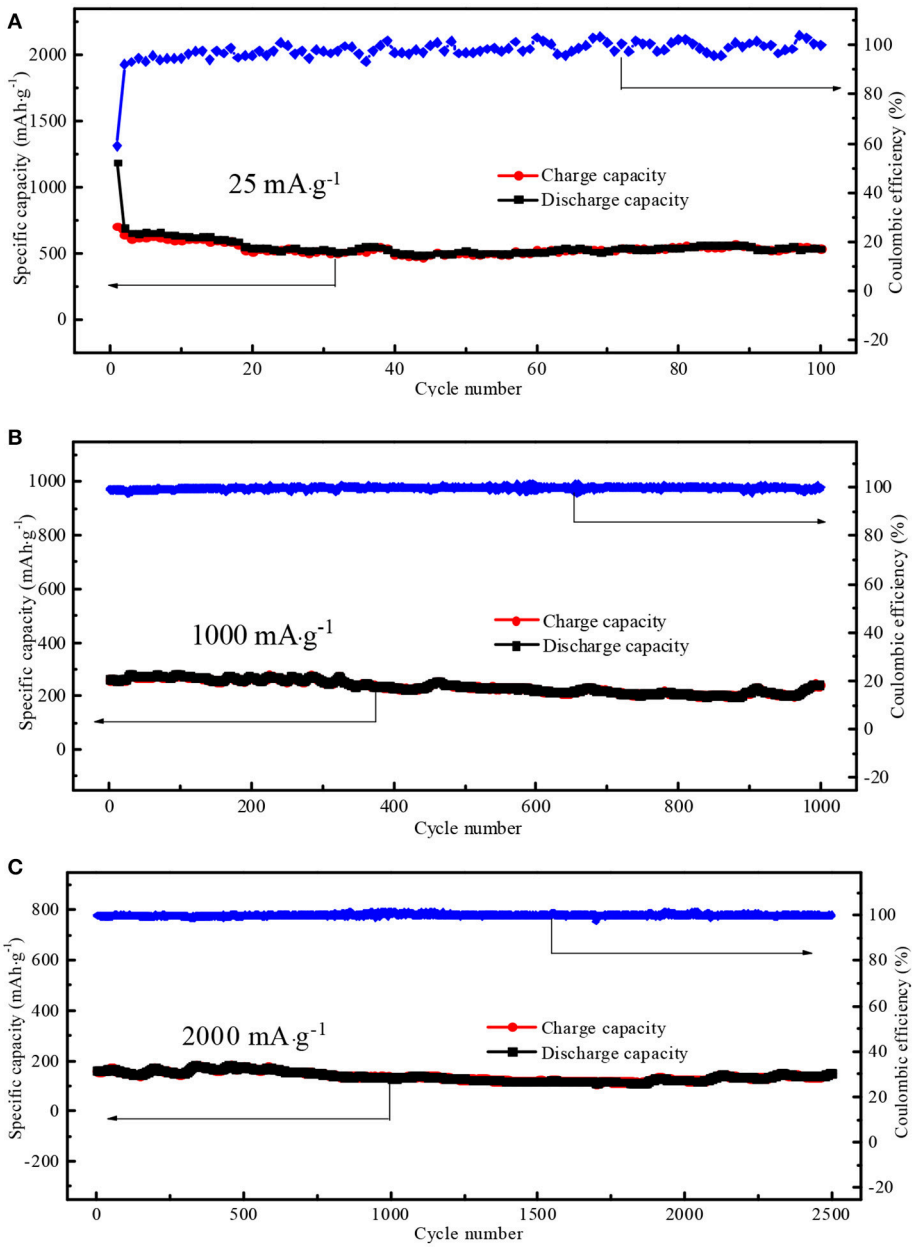

FIGURE 8 | The cycling performances of N-doped WCBC anode at **(A)** 25 mA·g^{-1}, **(B)** 1,000 mA·g^{-1}, and **(C)** 2,000 mA·g^{-1}.

co-existence of the micropores and mesopores (Qin and Chen, 2017). The pore size distribution plots were recorded from the desorption branch of the isotherms based on Barrett-Joyner-Halenda (BJH) model, as shown in **Figure 4B**. There existed five knee points at about 0.7, 2.7, 4.2, 5.6, and 7.3 nm in the pore size distribution curve, again indicating the co-existence of the micropores and the mesopores within N-doped WCBC powders (Hou et al., 2018). Furthermore, the surface area was calculated to be about 1,285 $m^2 \cdot g^{-1}$ according to Brunauer-Emmett-Teller (BET) equation at the range of P/P_0 = 0.05–0.23, higher than that of undoped carbon powders (Hou et al., 2018). No doubt, high specific surface area and multi-scaled pores can enlarge the electrode/electrolyte interface and facilitate the transport of Li^+ (Liu et al., 2016a; Zhang et al., 2017).

XPS Analysis

The fine chemical component of N-doped WCBC was further analyzed by XPS technology. As shown in the wide scan XPS spectrum in **Figure 5A**, three signal peaks were detected at 284.8, 399.6, and 532.0 eV, corresponding to C 1s, N 1s, and O 1s, respectively. The relative atomic percentages of C, N, and O were 90.8, 1.6, and 7.6%, respectively, indicating that N-doped WCBC powders consisted of major carbon and minor N-containing and O-containing functional groups. Furthermore, high resolution C1s spectrum could be deconvoluted into six peaks, among which one strong peak at 284.8 eV was assigned to C–C bond, while other five weak peaks at about 285.5, 286.2, 287.3, 288.8, and 290.6 eV were corresponding to C–N, C–O, C=N, C=O, and O=C-O bonds, respectively (**Figure 5B**) (Li and Xue, 2014; Selvamani et al., 2016; Liu et al., 2018). Moreover, three characteristic peaks were observed at 398.5, 400.2, and 401.4 eV in N1s spectrum in **Figure 5C**, corresponding to pyridinic N, pyrrolic N and quaternary N, respectively (Li and Xue, 2014; Hou et al., 2016). It was reported that pyrrolic N and pyridinic N may offer the additional active sites for Li-storage, thereby enhancing Li-storage capacity (Zheng et al., 2014). In the case of O 1s spectrum in **Figure 5D**, four peaks at 531.0, 532.3, 533.5, and 535.7 eV can be attributed to C=O, C–O, O=C–O, and H_2O, respectively (Saravanan and Kalaiselvi, 2015; Liu et al., 2016b). The residual O-containing functional groups (C=O, C–O, and O=C–O) may also increase the defects, the disorder or the local electron density beneficial for Li-storage, as reported elsewhere (Bhattacharjya et al., 2014). Seemingly, both N-doping and residual O-containing groups may play an important role in improving the electrochemical performances.

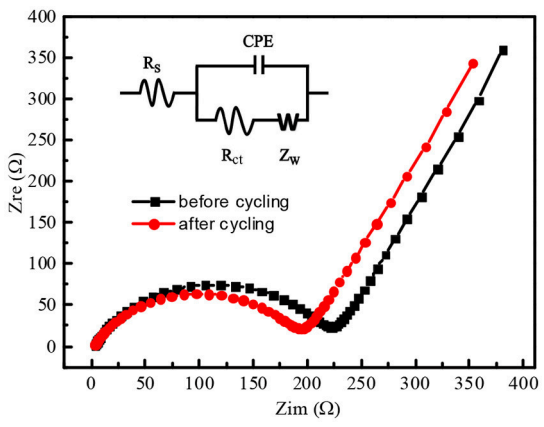

FIGURE 9 | Nyquist plots of N-doped WCBC anode, the inset: the corresponding equivalent circuit.

TABLE 1 | The fitting parameters of the equivalent circuit.

Parameters	Before cycling	After cycling
R_s (Ω)	2.58	2.59
R_{ct} (Ω)	221.30	192.60
Z_w (Ω)	2,233	2,095
i_0 ($mA \cdot cm^{-2}$)	0.10	0.12

Electrochemical Performances

Charge/Discharge Performances

Several representative charge/discharge profiles of N-doped WCBC anode at 25 $mA \cdot g^{-1}$ were shown in **Figure 6**. The corresponding specific discharge capacities at the 2nd, 20th, 80th, and 100th cycles were about 1,182, 686, 532, 531, and 528 $mAh \cdot g^{-1}$, respectively. Although there existed an initial irreversible capacity loss due to the formation of solid electrolyte interface (SEI) film, N-doped WCBC anode began to stably charge /discharge from the 20th cycle, indicating high reversibility (Bhattacharjya et al., 2014). Several possible reasons were responsible for the satisfactory charge/discharge performances: (i) N atoms within carbon matrix may act as the electron donors and increase the local state density at Fermi level, and thus improve the electronic conductivity and the charge transport; (ii) N-doping-induced pyridinic N and pyrrolic N species may provide the additional active sites for Li-storage; (iii) The existences of N and O atoms may also induce the formation of some defects, because the incorporation of the heteroatoms into the graphite-like lattice may promote the formation of some pentagons and thus the distortion of the graphite layer; (iv) the residual O-containing functional groups such as C=O, C–O, and O=C–O may also produce lots of radicals on the electrode surface and thus significantly enhance Li-storage by forming the chemical bonds with Li^+; (v) N-doping and O-containing groups may also induce the pseudo-capacitive Li-storage mechanisms, beneficial for the electrochemical performances; (vi) high specific surface area and multi-scaled pores can also enlarge the electrode/electrolyte interface and facilitate the ionic transport (Royea et al., 2006; Ismagilov et al., 2009; Wiggins-Camacho and Stevenson, 2009; Lee et al., 2011; Wang et al., 2012; Bhattacharjya et al., 2014; Zheng et al., 2014; Saravanan and Kalaiselvi, 2015).

CV Analysis

In order to further monitor the electrochemical behaviors of N-doped WCBC anode, CV measurement was also conducted at the different cycles, as shown in **Figure 7**. At the first cycle, an

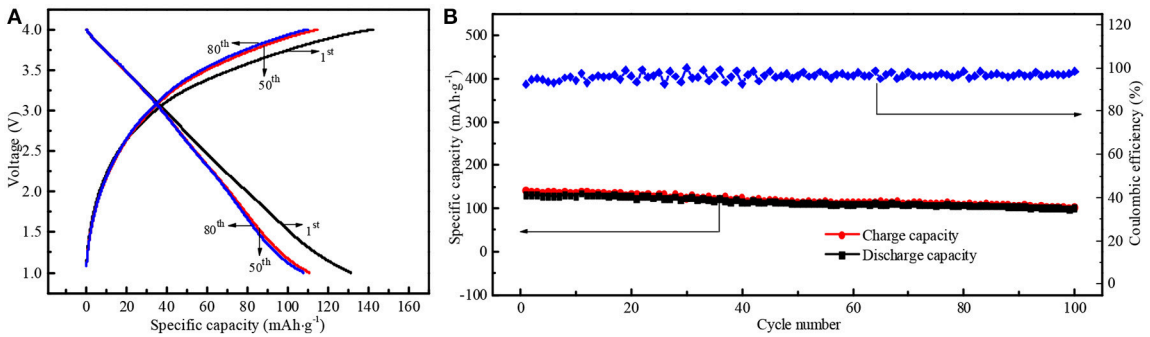

FIGURE 10 | (A) The 1st, 50th, and 80th galvanostatic charge/discharge profiles and **(B)** the cyclic performance of N-doped WCBC/$LiCoO_2$ full cell.

oxidation peak appeared at 0.25 V, while two reduction peaks were also detected at 0 and 0.7 V, respectively. Obviously, the oxidation peak corresponded to Li^+ deinsertion from N-doped WCBC anode, while the reduction peak at 0 V corresponded to Li^+ insertion into N-doped WCBC anode, and another reduction peak at 0.7 V was primarily attributed to the formation of SEI film (Wang et al., 2015; Mullaivananathan et al., 2017; Zhang et al., 2017). Subsequently, the reduction peak at about 0.7 V disappeared, and CV curve at the 2nd cycle almost overlapped with that at the 3rd cycle, indicating high reversibility of N-doped WCBC anode (Hou et al., 2018).

Cycling Performances

The cycling performances of N-doped WCBC anode were also shown in **Figure 8**. On cycling at 25 $mA{\cdot}g^{-1}$ after 100 cycles, a stable discharge capacity of 528 $mAh{\cdot}g^{-1}$ was maintained with 98% Coulombic efficiency (**Figure 8A**). Especially, the reversible discharge capacities remained about 241 and 151 $mAh{\cdot}g^{-1}$ even at 1,000 $mA{\cdot}g^{-1}$ for 1,000 cycles and 2,000 $mA{\cdot}g^{-1}$ for 2,500 cycles, respectively (in **Figure 8B** and **Figure 8C**). The corresponding capacity retentions were 94 and 92%, respectively, while both Coulombic efficiencies were 100%, demonstrating good electrochemical reversibility and long cycle life span of N-doped WCBC anode (Hou et al., 2018).

AC Impedance Analysis

Figure 9 showed Nyquist plots of N-doped WCBC anode before and after the cycling performances, and the corresponding equivalent circuit was also inset. Here, R_s, R_{ct}, CPE, and Z_w stand for the internal resistance, the charge transfer resistance, the double layer capacitance and Warburg impedance, respectively (Meng et al., 2016). After the cycling, R_s didn't change significantly, while R_{ct} and Z_w decreased, indicating that the charge transfer rate increased upon the cycling, as listed in **Table 1**. Additionally, the exchange current density (i_0) can be calculated according to Equation (1) (Elizabeth et al., 2016):

$$i_0 = RT/(nFR_{ct}A) \quad (1)$$

Where R is the ideal gas constant, T is the absolute temperature, F is Faraday constant, and A is the electrode area (about 1.1 cm^2) (Duan et al., 2016). Obviously, i_0 also increased upon the cycling, indicating facile charge transfer rate (Ou et al., 2015).

Full Cell Performances

To further investigate the practical feasibility of N-doped WCBC anode in LIB, a full cell was also assembled by coupling N-doped WCBC anode with commercial $LiCoO_2$ cathode. The 1st, 50th, and 80th galvanostatic charge/discharge profiles at 1.0–4.0 V were shown in **Figure 10A**. At the 1st cycle, the initial discharge capacity and Coulombic efficiency were about 131 $mAh{\cdot}g^{-1}$ and 92%, respectively. Subsequently, the corresponding discharge specific capacity slightly decreased to about 111 $mAh{\cdot}g^{-1}$ at the 50th cycle, close to that at the 80th cycle, indicating good cyclic stability, which was more intuitive and clear in **Figure 10B**. The reversible discharge specific capacity can maintain at 111 $mAh{\cdot}g^{-1}$ with 97% Coulombic efficiency, comparable with that of hard carbon/$LiCoO_2$ full cell in literature (Sun et al., 2007). Obviously, N-doped WCBC/$LiCoO_2$ full cell also exhibited good electrochemical performances, indicating high feasibility of N-doped WCBC anode in LIB.

CONCLUSIONS

In this work, the waste cigarette butts were recycled in form of N-doped carbon powders via one step facile carbonization. To be satisfactory, the resultant N-doped WCBC anode exhibited high reversible capacities of about 528 at 25 $mA{\cdot}g^{-1}$ for 100 cycles and about 151 $mAh{\cdot}g^{-1}$ even at 2,000 $mA{\cdot}g^{-1}$ for 2,500 cycles. N-doping effect such as high electronic conductivity, structural defects and additional active sites may contribute into the satisfactory electrochemical performances. Additionally, high specific surface area and the residual O-containing groups also facilitated high electrochemical performances. These satisfactory electrochemical performances may offer good inspiration and strategy to develop the sustainable energy and circular economy.

AUTHOR CONTRIBUTIONS

HH contributed to the conception and highlighted the scientific value of the study. CY and HH contributed significantly to analysis and manuscript preparation. HH and CY performed the

data analyses and wrote the manuscript. XL, LH, YY, ZD, and DL helped perform the analysis with with constructive discussions.

ACKNOWLEDGMENTS

This work was financially supported by the National Natural Science Foundations of China (Grant No. 51566006 and 51363011), the 46th Scientific Research Foundation for the Returned Overseas Chinese Scholars, State Education Ministry in China (6488-20130039), the 19th Young Academic and Technical Leaders of Yunnan Province (1097-10978240), the Program of High-level Introduced Talent of Yunnan Province (10978125), and the Project of Key Discipline (14078232 and 140 78311).

REFERENCES

Bhattacharjya, D., Park, H. Y., Kim, M. S., Choi, H. S., Inamdar, S. N., and Yu, J. S. (2014). Nitrogen-doped carbon nanoparticles by flame synthesis as anode material for rechargeable lithium-ion batteries. *Langmuir* 30, 318–324. doi: 10.1021/la403366e

Bulusheva, L. G., Okotrub, A. V., Kurenya, A. G., Zhang, H. K., Zhang, H. J., Chen, X. H., et al. (2011). Electrochemical properties of nitrogen-doped carbon nanotube anode in Li-ion batteries. *Carbon* 49, 4013–4023. doi: 10.1016/j.carbon.2011.05.043

Dai, D. M., Li, B., Tang, H. W., Chang, K., Jiang, K., Chang, Z. R., et al. (2016). Simultaneously improved capacity and initial coulombic efficiency of Li-rich cathode $Li[Li_{0.2}Mn_{0.54}Co_{0.13}Ni_{0.13}]O_2$ by enlarging crystal cell from a nanoplate precursor. *J. Power Sources* 307, 665–672. doi: 10.1016/j.jpowsour.2016.01.046

Duan, J. X., Hou, H. Y., Liu, X. X., Liu, S., Liao, Q. S., and Yao, Y. (2016). High performance PPO/Ti^{3+}/TiO_2NT membrane/electrode for lithium ion battery. *Ceram. Int*. 42, 16611–16618. doi: 10.1016/j.ceramint.2016.07.082

Elizabeth, I., Singh, B. P., Trikha, S., and Gopukumar, S. (2016). Bio-derived hierarchically macro-meso-micro porous carbon anode for lithium/sodium ion batteries. *J. Power Sources* 329, 412–421. doi: 10.1016/j.jpowsour.2016.08.106

Guernsey Police (2013). *Guernsey Police Issue Fixed Penalty Notices for Littering*. Available online at: http://www.sustainableguernsey.info/blog/2013/05/guernsey-police-issue-fixed-penalty-notices-for-littering

Han, P. X., Yue, Y. H., Zhang, L. X., Xu, H. X., Liu, Z. H., Zhang, K. J., et al. (2012). Nitrogen-doping of chemically reduced mesocarbon microbead oxide for the improved performance of lithium ion batteries. *Carbon* 50, 1355–1362. doi: 10.1016/j.carbon.2011.11.007

Hoffmann, D., and Hoffmann, I. (1997). The changing cigarette, 1950-1995. *J. Toxicol. Environ. Heal.* 50, 307–364. doi: 10.1080/009841097160393

Hou, H. Y., Liu, X. X., and Peng, J. H. (2016). "New Energe Material: Graphene," in *Graphene Science Handbook*, eds M. Aliofkhazraei, N. Ali, W. I. Milne, C. S. Ozkan, S. Mitura, and J. L. Gervasoni (Boca Raton, FL: CRC), 419–438.

Hou, H. Y., Yu, C. Y., Liu, X. X., Yao, Y., Liao, Q. S., Dai, Z. P., et al. (2018). Waste-loofah-derived carbon micro/nanoparticles for lithium ion battery anode. *Surf. Innov*. 6, 159–166. doi: 10.1680/jsuin.17.00068

Islami, F., Torre, L. A., and Jemal, A. (2015). Global trends of lung cancer mortality and smoking prevalence. *Transl. Lung Cancer Res.* 4, 327–338. doi: 10.3978/j.issn.2218-6751.2015.08.04

Ismagilov, Z. R., Shalagina, A. E., Podyacheva, O. Y., Ischenko, A. V., Kibis, L. S., Boronin, A. I., et al. (2009). Structure and electrical conductivity of nitrogen-doped carbon nanofibers. *Carbon* 47, 1922–1929. doi: 10.1016/j.carbon.2009.02.034

Jarvis, M. J. (2004). Why people smoke. *Brit. Med. J.* 328, 277–279. doi: 10.1136/bmj.328.7434.277

Jiang, Q., Zhang, Z. H., Yin, S. Y., Guo, Z. P., Wang, S. Q., and Feng, C. Q. (2016). Biomass carbon micro/nano-structures derived from ramie fibers and corncobs as anode materials for lithium-ion and sodium-ion batteries. *Appl. Surf. Sci.* 379, 73–82. doi: 10.1016/j.apsusc.2016.03.204

Lee, S. W., Gallant, B. M., Byon, H. R., Hammond, P. T., and Shao-Horn, Y. (2011). Nanostructured carbon-based electrodes: bridging the gap between thin-film lithium-ion batteries and electrochemical capacitors. *Energy Environ. Sci*. 4, 1972–1985. doi: 10.1039/C0EE00642D

Li, B., Li, Y. J., Dai, D. M., Chang, K., Tang, H. W., Chang, Z. R., et al. (2015). Facile and nonradiation pretreated membrane as a high conductive separator for Li-ion batteries. *ACS Appl. Mater. Interfaces* 7, 20184–20189. doi: 10.1021/acsami.5b05718

Li, B., Wei, X. G., Chang, Z. R., Chen, X. N., Yuan, X. Z., and Wang, H. J. (2014). Facile fabrication of $LiMn_2O_4$ microspheres from multi-shell MnO_2 for high-performance lithium-ion batteries. *Mater. Lett*. 135, 75–78. doi: 10.1016/j.matlet.2014.07.117

Li, M., and Xue, J. M. (2014). Integrated synthesis of nitrogen-doped mesoporous carbon from melamine resins with superior performance in supercapacitors. *J. Phys. Chem. C* 118, 2507–2517. doi: 10.1021/jp410198r

Liu, S., Hou, H. Y., Liu, X. X., Duan, J. X., Yao, Y., Liao, Q. S., et al. (2016a). Recycled hierarchical tripod-like CuCl from Cu-PCB waste etchant for lithium ion battery anode. *J. Hazard. Mater*. 324,357–364. doi: 10.1016/j.jhazmat.2016.10.069

Liu, S., Wang, G., Hou, H. Y., Liu, X. X., Duan, J. X., and Liao, Q. S. (2016b). Binder-free combination of large area reduced graphene oxide nanosheets with Cu foil for lithium ion battery anode. *Diam. Relat. Mater*. 68,102–108. doi: 10.1016/j.diamond.2016.06.013

Liu, X. F., Wang, D., Zhang, B. S., Luan, C., Qin, T. T., Zhang, W., et al. (2018). Vertical graphene nanowalls coating of copper current collector for enhancing rate performance of graphite anode of Li ion battery: the merit of optimized interface architecture. *Electrochim. Acta* 268, 234–240. doi: 10.1016/j.electacta.2018.02.004

Luo, J. S., Jensen, A. H., Brooks, N. R., Sniekers, J., Knipper, M., Aili, D., et al. (2015). 1,2,4-Triazolium perfluorobutanesulfonate as an archetypal pure protic organic ionic plastic crystal electrolyte for all-solid-state fuel cells. *Energy Environ. Sci*. 8, 1276–1291. doi: 10.1039/C4EE02280G

Meng, R. J., Hou, H. Y., Liu, X. X., Yan, C. X., Duan, J. X., and Liu, S. (2016). High performance binder-free quaternary composite CuO/Cu/TiO_2NT/Ti anode for lithium ion battery. *Ceram. Int*. 42, 6039–6045. doi: 10.1016/j.ceramint.2015.12.160

Mullaivananathan, V., Sathish, R., and Kalaiselvi, N. (2017). Coir pith derived bio-carbon: demonstration of potential anode behavior in lithium-ion batteries. *Electrochim. Acta* 225, 143–150. doi: 10.1016/j.electacta.2016.12.086

Ou, J. K., Zhang, Y. Z., Chen, L., Zhao, Q., Meng, Y., Guo, Y., et al. (2015). Nitrogen-rich porous carbon derived from biomass as a high performance anode material for lithium ion batteries. *J. Mater. Chem. A* 3, 6534–6541. doi: 10.1039/C4TA06614F

Qin, D., and Chen, S. (2017). A sustainable synthesis of biomass carbon sheets as excellent performance sodium ion batteries anode. *J. Solid State Electrochem*. 21, 1305–1312. doi: 10.1007/s10008-016-3485-z

Royea, W. J., Hamann, T. W., Brunschwig, B. S., and Lewis, N. S. (2006). A comparison between interfacial electron-transfer rate constants at metallic and graphite electrodes. *J. Phys. Chem. B* 110, 19433–19442. doi: 10.1021/jp062141e

Saravanan, K. R., and Kalaiselvi, N. (2015). Nitrogen containing bio-carbon as a potential anode for lithium batteries. *Carbon* 81, 43–53. doi: 10.1016/j.carbon.2014.09.021

Selvamani, V., Ravikumar, R., Suryanarayanan, V., Velayutham, D., and Gopukumar, S. (2016). Garlic peel derived high capacity hierarchical N-doped porous carbon anode for sodium/lithium ion cell. *Electrochim. Acta* 190, 337–345. doi: 10.1016/j.electacta.2016.01.006

Slaughter, E., Gersberg, R. M., Watanabe, K., Rudolph, J., Stransky, C., and Novotny, T. E. (2011). Toxicity of cigarette butts, and their chemical components, to marine and freshwater fish. *Tob. Control* 20, i25–i29. doi: 10.1136/tc.2010.040170

Smith, E. A., and Novotny, T. E. (2011). Whose butt is it? tobacco industry research about smokers and cigarette butt waste. *Tob. Control* 20, i2–i9. doi: 10.1136/tc.2010.040105

Song, H. W., Li, N., Cui, H., and Wang, C. X. (2014). Enhanced storage capability and kinetic processes by pores- and hetero-atoms-riched carbon nanobubbles for lithium-ion and sodium-ion batteries anodes. *Nano Energy* 4, 81–87. doi: 10.1016/j.nanoen.2013.12.017

Stephan, O., Ajayan, P. M., Colliex, C., Redlich, P., Lambert, J. M., Bernier, P., et al. (1994). Doping graphitic and carbon nanotube structures with boron and nitrogen. *Science* 266, 1683–1685. doi: 10.1126/science.266.5191.1683

Sun, H., He, X. M., Ren, J. G., Li, J. J., Jiang, C. Y., and Wan, C. R. (2007). Hard carbon/lithium composite anode materials for Li-ion batteries. *Electrochim. Acta* 52, 4312–4316. doi: 10.1016/j.electacta.2006.12.012

Thommes, M., Kaneko, K., Neimark, A. V., Olivier, J. P., Rodriguez-Reinoso, F., Rouquerol, J., et al. (2015). Physisorption of gases, with special reference to the evaluation of surface area and pore size distribution (IUPAC Technical Report). *Pure Appl. Chem*. 87, 1051–1069. doi: 10.1515/pac-2014-1117

Tie, X. Y., Han, Q. Y., Liang, C. Y., Li, B., Zai, J. T., and Qian, X. F. (2018). Si@SiOx/Graphene nanosheets composite: ball milling synthesis and enhanced lithium storage performance. *Front. Mater*. 4, 1–7. doi: 10.3389/fmats.2017.00047

Wang, F. F., Song, R. R., Song, H. H., Chen, X. H., Zhou, J. S., Ma, Z. K., et al. (2015). Simple synthesis of novel hierarchical porous carbon microspheres and their application to rechargeable lithium-ion batteries. *Carbon* 81, 314–321. doi: 10.1016/j.carbon.2014.09.062

Wang, H. B., Maiyalagan, T., and Wang, X. (2012). Review on recent progress in nitrogen-doped graphene: synthesis, characterization, and its potential applications. *ACS Catal*. 2, 781–794. doi: 10.1021/cs200652y

Wiggins-Camacho, J. D., and Stevenson, K. J. (2009). Effect of nitrogen concentration on capacitance, density of states, electronic conductivity, and morphology of N-doped carbon nanotube electrodes. *J. Phys. Chem. C* 113, 19082–19090. doi: 10.1021/jp907160v

Woods, S. (2015). *Help Local Councils Take Action Against Littering From Vehicles.* Available online at: http://www.slwoods.co.uk/?m=201505

Yu, C. Y., Hou, H. Y., Liu, X. X., Yao, Y., Liao, Q. S., Dai, Z. P., et al. (2018). Old-loofah-derived hard carbon for long cyclicity anode in sodium ion battery. *Int. J. Hydrogen Energy* 43, 3253–3260. doi: 10.1016/j.ijhydene.2017.12.151

Zhang, J. L., Zhang, L. J., Yang, S. L., Li, D. H., Xie, Z. X., Wang, B. B., et al. (2017). Facile strategy to produce N-doped carbon aerogels derived from seaweed for lithium-ion battery anode. *J. Alloys Compd*. 701, 256–261. doi: 10.1016/j.jallcom.2017.01.082

Zheng, F., Yang, Y., and Chen, Q. (2014). High lithium anodic performance of highly nitrogen-doped porous carbon prepared from a metal-organic framework. *Nat. Commun*. 5, 5261–5270. doi: 10.1038/ncomms6261

Conflict of Interest Statement: The authors declare that the research was conducted in the absence of any commercial or financial relationships that could be construed as a potential conflict of interest.